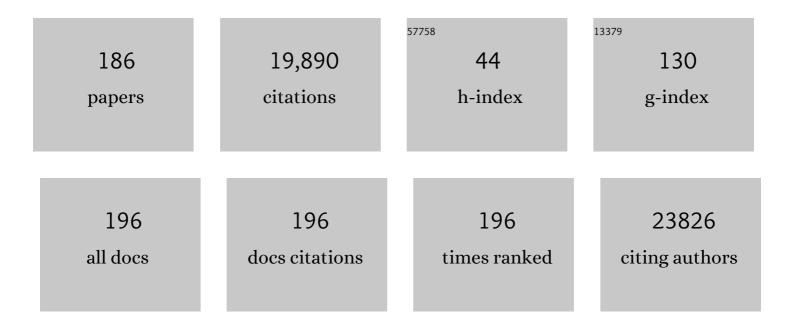
Paul A Yushkevich

List of Publications by Year in descending order

Source: https://exaly.com/author-pdf/1697767/publications.pdf Version: 2024-02-01



#	Article	IF	CITATIONS
1	Automatic Segmentation of Bone Selective MR Images for Visualization and Craniometry of the Cranial Vault. Academic Radiology, 2022, 29, S98-S106.	2.5	2
2	Tau pathology mediates age effects on medial temporal lobe structure. Neurobiology of Aging, 2022, 109, 135-144.	3.1	8
3	Fully Automated Placental Volume Quantification From <scp>3D</scp> Ultrasound for Prediction of Smallâ€forâ€Gestationalâ€Age Infants. Journal of Ultrasound in Medicine, 2022, 41, 1509-1524.	1.7	4
4	Ex vivo MRI and histopathology detect novel iron-rich cortical inflammation in frontotemporal lobar degeneration with tau versus TDP-43 pathology. NeuroImage: Clinical, 2022, 33, 102913.	2.7	17
5	Medial Temporal Lobe Networks in Alzheimer's Disease: Structural and Molecular Vulnerabilities. Journal of Neuroscience, 2022, 42, 2131-2141.	3.6	23
6	Dissociation of tau pathology and neuronal hypometabolism within the ATN framework of Alzheimer's disease. Nature Communications, 2022, 13, 1495.	12.8	11
7	Fully Automated 3D Segmentation and Diffeomorphic Medial Modeling of the Left Ventricle Mitral Valve Complex in Ischemic Mitral Regurgitation. Medical Image Analysis, 2022, 80, 102513.	11.6	1
8	Self- and Partner-Reported Subjective Memory Complaints: Association with Objective Cognitive Impairment and Risk of Decline. Journal of Alzheimer's Disease Reports, 2022, 6, 411-430.	2.2	4
9	Hippocampal subfield volumetry from structural isotropic 1 mm ³ <scp>MRI</scp> scans: A note of caution. Human Brain Mapping, 2021, 42, 539-550.	3.6	84
10	Multimodal image analysis and subvalvular dynamics in ischemic mitral regurgitation. JTCVS Open, 2021, 5, 48-60.	0.5	0
11	Cross-sectional and longitudinal medial temporal lobe subregional atrophy patterns in semantic variant primary progressive aphasia. Neurobiology of Aging, 2021, 98, 231-241.	3.1	5
12	Deep Label Fusion: A 3D End-To-End Hybrid Multi-atlas Segmentation and Deep Learning Pipeline. Lecture Notes in Computer Science, 2021, , 428-439.	1.3	1
13	Oh brother, where art tau? Amyloid, neurodegeneration, and cognitive decline without elevated tau. NeuroImage: Clinical, 2021, 31, 102717.	2.7	6
14	Accurate and Robust Alignment of Differently Stained Histologic Images Based on Greedy Diffeomorphic Registration. Applied Sciences (Switzerland), 2021, 11, 1892.	2.5	8
15	Early stages of tau pathology and its associations with functional connectivity, atrophy and memory. Brain, 2021, 144, 2771-2783.	7.6	78
16	Three-dimensional mapping of neurofibrillary tangle burden in the human medial temporal lobe. Brain, 2021, 144, 2784-2797.	7.6	38
17	Sensitive Measures of Cognition in Mild Cognitive Impairment. Journal of Alzheimer's Disease, 2021, 82, 1123-1136.	2.6	2
18	DeepAtrophy: Teaching a neural network to detect progressive changes in longitudinal MRI of the hippocampal region in Alzheimer's disease. NeuroImage, 2021, 243, 118514.	4.2	6

#	Article	IF	CITATIONS
19	Tauâ€Atrophy Variability Reveals Phenotypic Heterogeneity in Alzheimer's Disease. Annals of Neurology, 2021, 90, 751-762.	5.3	19
20	Ex vivo MRI atlas of the human medial temporal lobe: characterizing neurodegeneration due to tau pathology. Acta Neuropathologica Communications, 2021, 9, 173.	5.2	14
21	Early stages of tau pathology and its associations with functional connectivity, atrophy and memory. Alzheimer's and Dementia, 2021, 17, .	0.8	1
22	Regional distribution of tau pathology in subfields of hippocampus among phenotypic variants of AD and FTLD-tau Alzheimer's and Dementia, 2021, 17 Suppl 3, e052392.	0.8	0
23	Characterization of hippocampal subfields using ex vivo MRI and histology data: Lessons for in vivo segmentation. Hippocampus, 2020, 30, 545-564.	1.9	31
24	Quantitative threeâ€dimensional echocardiographic analysis of the bicuspid aortic valve and aortic root: A single modality approach. Journal of Cardiac Surgery, 2020, 35, 375-382.	0.7	0
25	Automated Meshing of Anatomical Shapes for Deformable Medial Modeling: Application to the Placenta in 3D Ultrasound. , 2020, , .		2
26	3D Mapping of TAU Neurofibrillary Tangle Pathology in the Human Medial Temporal Lobe. , 2020, , .		6
27	Building an Ex Vivo Atlas of the Earliest Brain Regions Affected by Alzheimer's Disease Pathology. , 2020, , .		3
28	Longitudinal atrophy in early Braak regions in preclinical Alzheimer's disease. Human Brain Mapping, 2020, 41, 4704-4717.	3.6	34
29	TAPAS: A Thresholding Approach for Probability Map Automatic Segmentation in Multiple Sclerosis. NeuroImage: Clinical, 2020, 27, 102256.	2.7	5
30	Intraoperative post-annuloplasty three-dimensional valve analysis does not predict recurrent ischemic mitral regurgitation. Journal of Cardiothoracic Surgery, 2020, 15, 161.	1.1	4
31	Neural and behavioral correlates of episodic memory are associated with temporal discounting in older adults. Neuropsychologia, 2020, 146, 107549.	1.6	16
32	ANHIR: Automatic Non-Rigid Histological Image Registration Challenge. IEEE Transactions on Medical Imaging, 2020, 39, 3042-3052.	8.9	75
33	Contribution of mixed pathology to medial temporal lobe atrophy in Alzheimer's disease. Alzheimer's and Dementia, 2020, 16, 843-852.	0.8	43
34	The Cancer Imaging Phenomics Toolkit (CaPTk): Technical Overview. Lecture Notes in Computer Science, 2020, 11993, 380-394.	1.3	34
35	Minimally interactive placenta segmentation from three-dimensional ultrasound images. Journal of Medical Imaging, 2020, 7, 1.	1.5	6
36	User-Guided Segmentation of Multi-modality Medical Imaging Datasets with ITK-SNAP. Neuroinformatics, 2019, 17, 83-102.	2.8	97

#	Article	IF	CITATIONS
37	Progress update from the hippocampal subfields group. Alzheimer's and Dementia: Diagnosis, Assessment and Disease Monitoring, 2019, 11, 439-449.	2.4	34
38	InÂvivo measures of tau burden are associated with atrophy in early Braak stage medial temporal lobe regions in amyloidâ€negative individuals. Alzheimer's and Dementia, 2019, 15, 1286-1295.	0.8	24
39	Structural and functional asymmetry of medial temporal subregions in unilateral temporal lobe epilepsy: A 7T MRI study. Human Brain Mapping, 2019, 40, 2390-2398.	3.6	49
40	Longitudinal Changes in Hippocampal Subfield Volume Associated with Collegiate Football. Journal of Neurotrauma, 2019, 36, 2762-2773.	3.4	20
41	Automated segmentation of medial temporal lobe subregions on in vivo T1â€weighted MRI in early stages of Alzheimer's disease. Human Brain Mapping, 2019, 40, 3431-3451.	3.6	71
42	Taskâ€enhanced arterial spin labeled perfusion MRI predicts longitudinal neurodegeneration in mild cognitive impairment. Hippocampus, 2019, 29, 26-36.	1.9	11
43	Associative memory for conceptually unitized word pairs in mild cognitive impairment is related to the volume of the perirhinal cortex. Hippocampus, 2019, 29, 630-638.	1.9	11
44	Improving Multi-atlas Segmentation by Convolutional Neural Network Based Patch Error Estimation. Lecture Notes in Computer Science, 2019, , 347-355.	1.3	5
45	Diffeomorphic Medial Modeling. Lecture Notes in Computer Science, 2019, 11492, 208-220.	1.3	Ο
46	Semi-automated Image Segmentation of the Midsystolic Left Ventricular Mitral Valve Complex in Ischemic Mitral Regurgitation. Lecture Notes in Computer Science, 2019, 11395, 142-151.	1.3	0
47	Early Tau Burden Correlates with Higher Rate of Atrophy in Transentorhinal Cortex. Journal of Alzheimer's Disease, 2018, 62, 85-92.	2.6	29
48	Longitudinal and cross-sectional structural magnetic resonance imaging correlates of AV-1451 uptake. Neurobiology of Aging, 2018, 66, 49-58.	3.1	61
49	Automated Multi-Atlas Segmentation of Hippocampal and Extrahippocampal Subregions in Alzheimer's Disease at 3T and 7T: What Atlas Composition Works Best?. Journal of Alzheimer's Disease, 2018, 63, 217-225.	2.6	11
50	Systematic comparison of different techniques to measure hippocampal subfield volumes in ADNI2. NeuroImage: Clinical, 2018, 17, 1006-1018.	2.7	56
51	Characterizing the human hippocampus in aging and Alzheimer's disease using a computational atlas derived from ex vivo MRI and histology. Proceedings of the National Academy of Sciences of the United States of America, 2018, 115, 4252-4257.	7.1	136
52	Mapping the structural and functional network architecture of the medial temporal lobe using 7T MRI. Human Brain Mapping, 2018, 39, 851-865.	3.6	60
53	Clinical validation of automated hippocampal segmentation in temporal lobe epilepsy. NeuroImage: Clinical, 2018, 20, 1139-1147.	2.7	14
54	Quantitative MRI of Perivascular Spaces at 3T for Early Diagnosis of Mild Cognitive Impairment. American Journal of Neuroradiology, 2018, 39, 1622-1628.	2.4	29

#	Article	IF	CITATIONS
55	Dice Overlap Measures for Objects of Unknown Number: Application to Lesion Segmentation. Lecture Notes in Computer Science, 2018, 10670, 3-14.	1.3	5
56	Joint Intensity Fusion Image Synthesis Applied to Multiple Sclerosis Lesion Segmentation. Lecture Notes in Computer Science, 2018, , 43-54.	1.3	3
57	Cancer imaging phenomics toolkit: quantitative imaging analytics for precision diagnostics and predictive modeling of clinical outcome. Journal of Medical Imaging, 2018, 5, 1.	1.5	110
58	Characterizing Anatomical Variability and Alzheimer's Disease Related Cortical Thinning in the Medial Temporal Lobe Using Graph-Based Groupwise Registration and Point Set Geodesic Shooting. Lecture Notes in Computer Science, 2018, 11167, 28-37.	1.3	4
59	Joint Intensity Fusion Image Synthesis Applied to Multiple Sclerosis Lesion Segmentation. , 2018, 10670, 43-54.		2
60	A protocol for manual segmentation of medial temporal lobe subregions in 7 Tesla MRI. NeuroImage: Clinical, 2017, 15, 466-482.	2.7	111
61	Spatiotemporal Segmentation and Modeling of the Mitral Valve in Real-Time 3D Echocardiographic Images. Lecture Notes in Computer Science, 2017, 10433, 746-754.	1.3	4
62	Gradient Boosted Trees for Corrective Learning. Lecture Notes in Computer Science, 2017, 10541, 203-211.	1.3	8
63	A tract-specific approach to assessing white matter in preterm infants. Neurolmage, 2017, 157, 675-694.	4.2	35
64	ITK-SNAP: An Intractive Medical Image Segmentation Tool to Meet the Need for Expert-Guided Segmentation of Complex Medical Images. IEEE Pulse, 2017, 8, 54-57.	0.3	96
65	Self-gated MRI of multiple beat morphologies in the presence of arrhythmias. Magnetic Resonance in Medicine, 2017, 78, 678-688.	3.0	9
66	A harmonized segmentation protocol for hippocampal and parahippocampal subregions: Why do we need one and what are the key goals?. Hippocampus, 2017, 27, 3-11.	1.9	130
67	Multi-template analysis of human perirhinal cortex in brain MRI: Explicitly accounting for anatomical variability. NeuroImage, 2017, 144, 183-202.	4.2	30
68	Medial temporal lobe subregional morphometry using high resolution MRI in Alzheimer's disease. Neurobiology of Aging, 2017, 49, 204-213.	3.1	70
69	Neural Correlates of Verbal Episodic Memory and Lexical Retrieval in Logopenic Variant Primary Progressive Aphasia. Frontiers in Neuroscience, 2017, 11, 330.	2.8	38
70	Image Segmentation and Modeling of the Pediatric Tricuspid Valve in Hypoplastic Left Heart Syndrome. Lecture Notes in Computer Science, 2017, 10263, 95-105.	1.3	17
71	Multiple Sclerosis Lesion Segmentation Using Joint Label Fusion. Lecture Notes in Computer Science, 2017, 10530, 138-145.	1.3	1
72	Maturation Along White Matter Tracts in Human Brain Using a Diffusion Tensor Surface Model Tract-Specific Analysis. Frontiers in Neuroanatomy, 2016, 10, 9.	1.7	37

#	Article	IF	CITATIONS
73	Automated Hippocampal Subfield Segmentation at 7T MRI. American Journal of Neuroradiology, 2016, 37, 1050-1057.	2.4	66
74	The value of preoperative 3-dimensional over 2-dimensional valve analysis in predicting recurrent ischemic mitral regurgitation after mitral annuloplasty. Journal of Thoracic and Cardiovascular Surgery, 2016, 152, 847-859.	0.8	26
75	ICâ€Pâ€174: Fast Automatic Segmentation of Hippocampal Subfields and Medial Temporal Lobe Subregions In 3 Tesla and 7 Tesla T2â€Weighted MRI. Alzheimer's and Dementia, 2016, 12, P126.	0.8	42
76	Quantification of Left Ventricular Function With Premature Ventricular Complexes Reveals Variable Hemodynamics. Circulation: Arrhythmia and Electrophysiology, 2016, 9, e003520.	4.8	20
77	Modeling the Myxomatous Mitral Valve With Three-Dimensional Echocardiography. Annals of Thoracic Surgery, 2016, 102, 703-710.	1.3	9
78	Globally Optimal Label Fusion with Shape Priors. Lecture Notes in Computer Science, 2016, 9901, 538-546.	1.3	5
79	A framework for informing segmentation of in vivo MRI with information derived from ex vivo imaging: Application in the medial temporal lobe. , 2016, 2016, 6014-6017.		2
80	Supervoxel-Based Hierarchical Markov Random Field Framework for Multi-atlas Segmentation. Lecture Notes in Computer Science, 2016, , 100-108.	1.3	0
81	ITK-SNAP: An interactive tool for semi-automatic segmentation of multi-modality biomedical images. , 2016, 2016, 3342-3345.		250
82	Clinical Application of Automatic Segmentation of Medial Temporal Lobe Subregions in Prodromal and Dementia-Level Alzheimer's Disease. Journal of Alzheimer's Disease, 2016, 54, 1027-1037.	2.6	9
83	A brain stress test: Cerebral perfusion during memory encoding in mild cognitive impairment. NeuroImage: Clinical, 2016, 11, 388-397.	2.7	30
84	In-vivo heterogeneous functional and residual strains in human aortic valve leaflets. Journal of Biomechanics, 2016, 49, 2481-2490.	2.1	32
85	Preoperative Three-Dimensional Valve Analysis Predicts Recurrent Ischemic Mitral Regurgitation After Mitral Annuloplasty. Annals of Thoracic Surgery, 2016, 101, 567-575.	1.3	53
86	Accounting for the Confound of Meninges in Segmenting Entorhinal and Perirhinal Cortices in T1-Weighted MRI. Lecture Notes in Computer Science, 2016, 9901, 564-571.	1.3	21
87	Probabilistic Atlas of the Human Hippocampus Combining Ex Vivo MRI and Histology. Lecture Notes in Computer Science, 2016, , 63-71.	1.3	2
88	ND morphological contour interpolation. The Insight Journal, 2016, , .	0.2	11
89	RLEImage: run-length encoded memory compression scheme for an itk::Image. The Insight Journal, 2016, , ·	0.2	1
90	User-initialized active contour segmentation and golden-angle real-time cardiovascular magnetic resonance enable accurate assessment of LV function in patients with sinus rhythm and arrhythmias. Journal of Cardiovascular Magnetic Resonance, 2015, 17, 37.	3.3	19

#	Article	IF	CITATIONS
91	Automated volumetry and regional thickness analysis of hippocampal subfields and medial temporal cortical structures in mild cognitive impairment. Human Brain Mapping, 2015, 36, 258-287.	3.6	454
92	Medially constrained deformable modeling for segmentation of branching medial structures: Application to aortic valve segmentation and morphometry. Medical Image Analysis, 2015, 26, 217-231.	11.6	26
93	Guest editorial. Neurobiology of Aging, 2015, 36, S1-S2.	3.1	1
94	Anterior and posterior MTL networks in aging and MCI. Neurobiology of Aging, 2015, 36, S141-S150.e1.	3.1	44
95	Quantitative comparison of 21 protocols for labeling hippocampal subfields and parahippocampal subregions in in vivo MRI: Towards a harmonized segmentation protocol. NeuroImage, 2015, 111, 526-541.	4.2	284
96	Relationship of Contextual Cueing and Hippocampal Volume in Amnestic Mild Cognitive Impairment Patients and Cognitively Normal Older Adults. Journal of the International Neuropsychological Society, 2015, 21, 285-296.	1.8	12
97	Multi-atlas label fusion with augmented atlases for fast and accurate segmentation of cardiac MR images. , 2015, , .		4
98	Suspected non-AD pathology in mild cognitive impairment. Neurobiology of Aging, 2015, 36, 3152-3162.	3.1	63
99	Assessing atrophy measurement techniques in dementia: Results from the MIRIAD atrophy challenge. NeuroImage, 2015, 123, 149-164.	4.2	63
100	Segmentation of the Aortic Valve Apparatus in 3D Echocardiographic Images: Deformable Modeling of a Branching Medial Structure. Lecture Notes in Computer Science, 2015, 8896, 196-203.	1.3	7
101	4D-transesophageal echocardiography and emerging imaging modalities for guiding mitral valve repair. Annals of Cardiothoracic Surgery, 2015, 4, 461-2.	1.7	4
102	White Matter Disease Contributes to Apathy and Disinhibition in Behavioral Variant Frontotemporal Dementia. Cognitive and Behavioral Neurology, 2014, 27, 206-214.	0.9	33
103	Real-Time Magnetic Resonance Imaging TechniqueÂfor Determining Left Ventricle Pressure-Volume Loops. Annals of Thoracic Surgery, 2014, 97, 1597-1603.	1.3	18
104	Histology-derived volumetric annotation of the human hippocampal subfields in postmortem MRI. NeuroImage, 2014, 84, 505-523.	4.2	133
105	Fully automatic segmentation of the mitral leaflets in 3D transesophageal echocardiographic images using multi-atlas joint label fusion and deformable medial modeling. Medical Image Analysis, 2014, 18, 118-129.	11.6	70
106	Statistical Assessment of Normal Mitral Annular Geometry Using Automated Three-Dimensional Echocardiographic Analysis. Annals of Thoracic Surgery, 2014, 97, 71-77.	1.3	25
107	Automatic Clustering and Thickness Measurement of Anatomical Variants of the Human Perirhinal Cortex. Lecture Notes in Computer Science, 2014, 17, 81-88.	1.3	9
108	Increased functional connectivity within medial temporal lobe in mild cognitive impairment. Hippocampus, 2013, 23, 1-6.	1.9	79

#	Article	IF	CITATIONS
109	White Matter Disease Correlates with Lexical Retrieval Deficits in Primary Progressive Aphasia. Frontiers in Neurology, 2013, 4, 212.	2.4	29
110	Multi-Atlas Segmentation with Joint Label Fusion. IEEE Transactions on Pattern Analysis and Machine Intelligence, 2013, 35, 611-623.	13.9	699
111	Multi-atlas segmentation with joint label fusion and corrective learning—an open source implementation. Frontiers in Neuroinformatics, 2013, 7, 27.	2.5	188
112	Deformable Modeling Using a 3D Boundary Representation with Quadratic Constraints on the Branching Structure of the Blum Skeleton. Lecture Notes in Computer Science, 2013, 23, 280-291.	1.3	12
113	Multi-atlas Segmentation with Robust Label Transfer and Label Fusion. Lecture Notes in Computer Science, 2013, 23, 548-559.	1.3	32
114	Multi-atlas Segmentation without Registration: A Supervoxel-Based Approach. Lecture Notes in Computer Science, 2013, 16, 535-542.	1.3	28
115	Automated Segmentation and Geometrical Modeling of the Tricuspid Aortic Valve in 3D Echocardiographic Images. Lecture Notes in Computer Science, 2013, 16, 485-492.	1.3	16
116	Groupwise Segmentation with Multi-atlas Joint Label Fusion. Lecture Notes in Computer Science, 2013, 16, 711-718.	1.3	17
117	Dependency prior for multi-atlas label fusion. , 2012, 2012, 892-895.		6
118	Fully automatic segmentation of the open mitral leaflets in 3D transesophageal echocardiographic images using multi-atlas label fusion and deformable medial modeling. , 2012, , .		0
119	Development of a semi-automated method for mitral valve modeling with medial axis representation using 3D ultrasound. Medical Physics, 2012, 39, 933-950.	3.0	29
120	In vivo Analysis of Hippocampal Subfield Atrophy in Mild Cognitive Impairment via Semi-Automatic Segmentation of T2-Weighted MRI. Journal of Alzheimer's Disease, 2012, 31, 85-99.	2.6	99
121	Dynamic shape modeling of the mitral valve from real-time 3D ultrasound images using continuous medial representation. , 2012, , .		0
122	Reconstruction of the human hippocampus in 3D from histology and high-resolution ex-vivo MRI. , 2012, 294-297.		7
123	Spatial bias in multi-atlas based segmentation. , 2012, 2012, 909-916.		10
124	From label fusion to correspondence fusion: A new approach to unbiased groupwise registration. , 2012, , 956-963.		14
125	Semi-automated mitral valve morphometry and computational stress analysis using 3D ultrasound. Journal of Biomechanics, 2012, 45, 903-907.	2.1	41
126	Measuring longitudinal change in the hippocampal formation from in vivo high-resolution T2-weighted MRI. NeuroImage, 2012, 60, 1266-1279.	4.2	35

#	Article	IF	CITATIONS
127	Robust Automated Amygdala Segmentation via Multi-Atlas Diffeomorphic Registration. Frontiers in Neuroscience, 2012, 6, 166.	2.8	28
128	White matter imaging contributes to the multimodal diagnosis of frontotemporal lobar degeneration. Neurology, 2012, 78, 1761-1768.	1.1	48
129	Guiding Automatic Segmentation with Multiple Manual Segmentations. Lecture Notes in Computer Science, 2012, 15, 429-436.	1.3	2
130	Regression-based label fusion for multi-atlas segmentation. , 2011, , 1113-1120.		49
131	A learning-based wrapper method to correct systematic errors in automatic image segmentation: Consistently improved performance in hippocampus, cortex and brain segmentation. NeuroImage, 2011, 55, 968-985.	4.2	162
132	Heterogeneity of functional activation during memory encoding across hippocampal subfields in temporal lobe epilepsy. Neurolmage, 2011, 58, 1121-1130.	4.2	18
133	Hippocampus segmentation using a stable maximum likelihood classifier ensemble algorithm. , 2011, , .		4
134	Optimal Weights for Multi-atlas Label Fusion. Lecture Notes in Computer Science, 2011, 22, 73-84.	1.3	32
135	N4ITK: Improved N3 Bias Correction. IEEE Transactions on Medical Imaging, 2010, 29, 1310-1320.	8.9	4,205
136	A tract-specific framework for white matter morphometry combining macroscopic and microscopic tract features. Medical Image Analysis, 2010, 14, 666-673.	11.6	52
137	Automatic Cardiac MRI Segmentation Using a Biventricular Deformable Medial Model. Lecture Notes in Computer Science, 2010, 13, 468-475.	1.3	26
138	3D mesh based wall thickness measurement: Identification of left ventricular hypertrophy phenotypes. , 2010, 2010, 2642-5.		7
139	Nearly automatic segmentation of hippocampal subfields in in vivo focal T2-weighted MRI. NeuroImage, 2010, 53, 1208-1224.	4.2	222
140	Cerebral cortical folding analysis with multivariate modeling and testing: Studies on gender differences and neonatal development. NeuroImage, 2010, 53, 450-459.	4.2	62
141	The optimal template effect in hippocampus studies of diseased populations. NeuroImage, 2010, 49, 2457-2466.	4.2	605
142	Bias in estimation of hippocampal atrophy using deformation-based morphometry arises from asymmetric global normalization: An illustration in ADNI 3 T MRI data. NeuroImage, 2010, 50, 434-445.	4.2	116
143	Standing on the Shoulders of Giants: Improving Medical Image Segmentation via Bias Correction. Lecture Notes in Computer Science, 2010, 13, 105-112.	1.3	5
144	Shape-based semi-automatic hippocampal subfield segmentation with learning-based bias removal. , 2010, , .		1

9

#	Article	IF	CITATIONS
145	A Computational White Matter Atlas for Aging with Surface-Based Representation of Fasciculi. Lecture Notes in Computer Science, 2010, , 83-90.	1.3	17
146	Structure specific analysis of the hippocampus in temporal lobe epilepsy. Hippocampus, 2009, 19, 517-525.	1.9	24
147	Hippocampal volumetry and functional MRI of memory in temporal lobe epilepsy. Epilepsy and Behavior, 2009, 16, 128-138.	1.7	35
148	Ventricularwall thickness analysis in acute myocardial infarction and hypertrophic cardiomyopathy. , 2009, , .		1
149	A high-resolution computational atlas of the human hippocampus from postmortem magnetic resonance imaging at 9.4ÂT. NeuroImage, 2009, 44, 385-398.	4.2	160
150	Continuous medial representation of brain structures using the biharmonic PDE. NeuroImage, 2009, 45, S99-S110.	4.2	37
151	Multivariate High-Dimensional Cortical Folding Analysis, Combining Complexity and Shape, in Neonates with Congenital Heart Disease. Lecture Notes in Computer Science, 2009, 21, 552-563.	1.3	18
152	A Tract-Specific Framework for White Matter Morphometry Combining Macroscopic and Microscopic Tract Features. Lecture Notes in Computer Science, 2009, 12, 141-149.	1.3	8
153	Tensor-Based Morphometry of Fibrous Structures with Application to Human Brain White Matter. Lecture Notes in Computer Science, 2009, 12, 466-473.	1.3	2
154	Structure-Specific Statistical Mapping of White Matter Tracts. Mathematics and Visualization, 2009, , 83-112.	0.6	4
155	Gender Differences in Cerebral Cortical Folding: Multivariate Complexity-Shape Analysis with Insights into Handling Brain-Volume Differences. Lecture Notes in Computer Science, 2009, 12, 200-207.	1.3	5
156	Live-Wire-ing the Insight Toolkit with Intelligent Scissors. The Insight Journal, 2009, , .	0.2	0
157	Structure-specific statistical mapping of white matter tracts. NeuroImage, 2008, 41, 448-461.	4.2	158
158	Building an atlas of hippocampal subfields using postmortem MRI. , 2008, , .		2
159	Branching medial models for cardiac shape representation. , 2008, , .		4
160	Surface-based modeling of white matter fasciculi with orientation encoding. , 2008, , .		1
161	Spatial correspondence based asymmetry analysis in FMRI. , 2008, , .		0
162	Shape-Based Alignment of Hippocampal Subfields: Evaluation in Postmortem MRI. Lecture Notes in Computer Science, 2008, 11, 510-517.	1.3	9

#	Article	IF	CITATIONS
163	3D Cerebral Cortical Morphometry in Autism: Increased Folding in Children and Adolescents in Frontal, Parietal, and Temporal Lobes. Lecture Notes in Computer Science, 2008, 11, 559-567.	1.3	22
164	Cardiac Medial Modeling and Time-Course Heart Wall Thickness Analysis. Lecture Notes in Computer Science, 2008, 11, 766-773.	1.3	12
165	High-Dimensional Spatial Normalization of Diffusion Tensor Images Improves the Detection of White Matter Differences: An Example Study Using Amyotrophic Lateral Sclerosis. IEEE Transactions on Medical Imaging, 2007, 26, 1585-1597.	8.9	250
166	Structure-Specific Statistical Mapping of White Matter Tracts using the Continuous Medial Representation. , 2007, , .		24
167	Hippocampus-specific fMRI group activation analysis using the continuous medial representation. NeuroImage, 2007, 35, 1516-1530.	4.2	28
168	Shape-Based Normalization of the Corpus Callosum for DTI Connectivity Analysis. IEEE Transactions on Medical Imaging, 2007, 26, 1166-1178.	8.9	18
169	Neuroinformatics for Genome-Wide 3-D Gene Expression Mapping in the Mouse Brain. IEEE/ACM Transactions on Computational Biology and Bioinformatics, 2007, 4, 382-393.	3.0	109
170	NON-UNIFORM SMOOTHING IN HIPPOCAMPUS-SPECIFIC GROUP FMRI ANALYSIS. , 2007, , .		0
171	Unbiased White Matter Atlas Construction Using Diffusion Tensor Images. , 2007, 10, 211-218.		66
172	Evaluation of Shape-Based Normalization in the Corpus Callosum for White Matter Connectivity Analysis. , 2007, 10, 777-784.		0
173	Continuous Medial Representation for Anatomical Structures. IEEE Transactions on Medical Imaging, 2006, 25, 1547-1564.	8.9	119
174	Deformable registration of diffusion tensor MR images with explicit orientation optimization. Medical Image Analysis, 2006, 10, 764-785.	11.6	453
175	User-guided 3D active contour segmentation of anatomical structures: Significantly improved efficiency and reliability. NeuroImage, 2006, 31, 1116-1128.	4.2	6,669
176	Hippocampus-Specific fMRI Group Activation Analysis with Continuous M-Reps. Lecture Notes in Computer Science, 2006, 9, 284-291.	1.3	1
177	Anatomy-Based Visualizations of Diffusion Tensor Images of Brain White Matter. Mathematics and Visualization, 2006, , 155-163.	0.6	3
178	Parametric Medial Shape Representation in 3-D via the Poisson Partial Differential Equation with Non-linear Boundary Conditions. Lecture Notes in Computer Science, 2005, 19, 162-173.	1.3	7
179	Regional Structural Characterization of the Brain of Schizophrenia Patients1. Academic Radiology, 2005, 12, 1250-1261.	2.5	20
180	Statistical Modeling of Shape and Appearance Using the Continuous Medial Representation. Lecture Notes in Computer Science, 2005, 8, 725-732.	1.3	6

#	Article	IF	CITATIONS
181	Deformable M-Reps for 3D Medical Image Segmentation. International Journal of Computer Vision, 2003, 55, 85-106.	15.6	202
182	Continuous medial representations for geometric object modeling in 2D and 3D. Image and Vision Computing, 2003, 21, 17-27.	4.5	59
183	Feature Selection for Shape-Based Classification of Biological Objects. Lecture Notes in Computer Science, 2003, 18, 114-125.	1.3	25
184	Multiscale deformable model segmentation and statistical shape analysis using medial descriptions. IEEE Transactions on Medical Imaging, 2002, 21, 538-550.	8.9	112
185	Intuitive, Localized Analysis of Shape Variability. Lecture Notes in Computer Science, 2001, , 402-408.	1.3	26
186	Segmentation, registration, and measurement of shape variation via image object shape. IEEE Transactions on Medical Imaging, 1999, 18, 851-865.	8.9	268